Elsevier Editorial System(tm) for
International Journal of Refrigeration
Manuscript Draft

Manuscript Number: JIJR-D-18-00584R1

Title: Investigation of an ejector powered double-effect absorption/recompression refrigeration cycle

Article Type: Research Paper

Keywords: Double-effect absorption/recompression cycle; Water/lithium bromide; Ejector; High temperature heat sources

Corresponding Author: Professor Mahmoud Bourouis, Ph.D.

Corresponding Author's Institution: Rovira i Virgili University

First Author: Doniazed Sioud, PhD Student

Order of Authors: Doniazed Sioud, PhD Student; Mahmoud Bourouis, Ph.D.; Ahmed Bellagi, PhD

Abstract: The objective of the present work is to investigate the feasibility and the eventual improvement in performance of an ejector powered water/lithium bromide double-effect absorption/recompression refrigeration cycle driven by high temperature heat sources.
The results show that the cycle performance parameters are significantly affected by the presence of the ejector and its characteristics. Further, the COP responses to variation of working conditions are different from those observed for the conventional double-effect absorption refrigeration cycles. The maximum COP values of the ejector cycle occur at HP-generator temperatures lower by 20°C to 25°C than those of the conventional double-effect absorption cycle. The enhancement factor of the COP varies between 1.34 and 1.70 at a driving steam temperature ranging from 240°C to 340°C. As regards the ejector design, the ratio of HP-generator pressure and driving steam pressure should be kept as low as possible. The geometry of the design should allow for the maximum entrainment ratio feasible.

Investigation of an ejector powered double-effect absorption/recompression refrigeration cycle

Doniazed Sioud[1], Mahmoud Bourouis[2*], Ahmed Bellagi[1]
[1]U.R. Thermique & Thermodynamique des Procédés Industriels
Ecole Nationale d'Ingénieurs de Monastir-ENIM, University of Monastir, Monastir, Tunisia

[2]Universitat Rovira i Virgili, Department of Mechanical Engineering
Av. Països Catalans No. 26, 43007Tarragona, Spain

***Corresponding author:**

Email: mahmoud.bourouis@urv.cat

Abstract

The objective of the present work is to investigate the feasibility and the eventual improvement in performance of an ejector powered water/lithium bromide double-effect absorption/recompression refrigeration cycle driven by high temperature heat sources.

The results show that the cycle performance parameters are significantly affected by the presence of the ejector and its characteristics. Further, the COP responses to variation of working conditions are different from those observed for the conventional double-effect absorption refrigeration cycles. The maximum COP values of the ejector cycle occur at HP−generator temperatures lower by 20ºC to 25ºC than those of the conventional double-effect absorption cycle. The enhancement factor of the COP varies between 1.34 and 1.70 at a driving steam temperature ranging from 240ºC to 340ºC. As regards the ejector design, the ratio of HP−generator pressure and driving steam pressure should be kept as low as possible. The geometry of the design should allow for the maximum entrainment ratio feasible.

Keywords:

- Double-effect absorption/recompression cycle
- Water/lithium bromide
- Ejector
- High temperature heat sources

1. Introduction

Absorption chillers are usually used in large-scale air-conditioning systems for both industrial and commercial applications, and also in heat recovery from industrial power plants. The most common working fluids used in these systems are water/lithium bromide and ammonia/water. The former is used only in air-conditioning applications, because water freezes at 0°C, and the latter mainly in refrigeration applications that require cooling below 0ºC. The efficiency of absorption cycles is usually assessed in terms of the coefficient of performance (COP), which is rather low for the single-effect configuration, namely around 0.7 for water/LiBr and 0.5 for ammonia/water. Hence, the improvement of the COP of absorption cooling cycles is an issue that is reported in several investigations in the open literature. The use of advanced configurations such as double and triple-effect cycles is one way to increase the efficiency of these cooling cycles.

In this context, some investigations proposed instead the integration of an ejector into absorption cooling systems. Two alternative locations of the ejector in single-effect cycles were discussed: between the generator and the evaporator and between the evaporator and the absorber. Several authors investigated the first arrangement. Sun et al. [1] and Majdi [2] theoretically explored the ejector water/lithium bromide single-effect absorption cycle using different geometries for the ejector. They concluded that the COP of the ejector absorption cycle is higher than that of the conventional absorption cycle. Jiang et al. [3] compared the coefficient of performance of the ejector single-effect absorption cycle with that of small capacity water/lithium bromide double-effect absorption chillers. The authors reported that the COP of the ejector absorption cycle was up to 0.9–1.0, just slightly below that of the commercial double-effect absorption chillers. Aphornratana et al. [4] carried out an experimental study on a three-pressure ejector absorption refrigeration machine and showed that the COP of the ejector absorption machine was 30–60% higher than that of the basic single-effect absorption cycle and achieved the COP of small commercial double-effect absorption refrigeration machines. In the literature on ammonia/water ejector absorption refrigeration systems, it is reported that higher values of the coefficient of performance can be achieved by adding a flash tank between the ejector and the evaporator. Hence, Sirwan et al. [5] and Abed et al. [6] carried out a theoretical study to analyse the effect of the flash tank on the entertainment ratio and the cycle performances. Their results showed that this cycle configuration (ejector and flash tank) improved the coefficient of performance. This was

because the increase in the amount of refrigerant delivered to the evaporator coming from the flash tank increased the cooling effect.

Other researchers investigated the second configuration in which the ejector is located at the absorber entrance and replaced the solution expansion valve. Shi et al. [7] explored this arrangement for heat transformers using water/lithium bromide as a working pair, and Sözen et al. [8] using ammonia/water. Their results showed that the new design was simpler than that of the two-stage heat transformer and double absorption heat transformer (where a pump and an absorber/evaporator are added to a single-stage heat transformer). The delivered useful temperature was higher than in the case of a single-stage heat transformer, and the COP improved [7]. Vereda et al. [9] evaluated the feasibility of an adjustable nozzle area in an ejector absorption refrigerator using ammonia/lithium nitrate. They reported that the activation temperature was reduced by about 9°C on integrating the ejector, and the COP increased at moderate temperatures, particularly when the temperature of the driving hot water inlet generator was lower than 81-92°C. Garousi Farshi et al. [10] compared the results obtained by Vereda et al. [9] with those of the ammonia/NaSCN ejector absorption cycles. They concluded that both COP and exergy efficiency were higher than in single-effect absorption refrigeration cycles especially at low generator temperatures.

An advanced configuration, reported in the literature for ejector absorption refrigeration cycles, consists of coupling the ejector with the solution generator via an external loop. This involved a steam generator and a steam ejector which compressed the vapour desorbed from the water/lithium bromide solution in order to re-heat the solution in the desorber. Thus, Eames and Wu [11] described the configuration of an ejector powered water/lithium bromide single-effect absorption/recompression refrigeration cycle and theoretically investigated its energy efficiency and performance characteristics. Their results showed that the COP of the cycle increased with the temperature of the driving heat. Eames and Wu [12] and Wu and Eames [13] also investigated experimentally a 5 kW re-compression refrigerator prototype. The coefficient of performance (COP) of this prototype was 1.03 at the design operating conditions, which was 14% lower than that of the estimated theoretical value. However, it was higher than that of the single-effect absorption chiller and close to the typical value of the conventional double-effect absorption cycle. The authors concluded that the ejector absorption refrigeration cycle was an efficient configuration when a high temperature heat source is available.

The integration of ejectors into more elaborated configurations of absorption cooling cycles was also considered. Hong et al. [14] investigated a parallel-flow double-effect ejector absorption cycle. Compared to the basic configuration of the single-effect absorption cycle, their results showed that the COP improved by 10%, 20% and 30% when the heat source temperature was set at 130ºC, 136ºC and 142°C, respectively. Moreover, at heat source temperatures higher than 122°C and lower than 150ºC, the efficiency of the ejector double-effect absorption cycle was better than that of the conventional double-effect absorption cycle. Farshi et al. [15] investigated an ejector series-flow double-effect absorption refrigeration cycle. The authors performed a thermodynamic analysis comparing their cycle with the single-effect and series-flow double-effect absorption cycles. They concluded that at a particular range of the heat source temperature between 92ºC and 137°C, the proposed cycle operated more efficiently than the two other cycles.

For heat sources at temperatures over 170ºC, the triple-effect configuration of the absorption cycle was investigated by several researchers. Grossman and Wilk [16, 17] compared the theoretical performances of parallel-flow and series-flow triple-effect water/lithium bromide absorption chillers. In both cases, heat from external source was supplied solely to the HP–generator; each intermediate-pressure generator was powered by heat rejected by the next high temperature condenser. In the configuration of series-connected generators, the aqueous salt solution exiting the absorber fed successively the low-pressure generator, then the intermediate-pressure generator and finally the HP–generator. In the parallel-connected arrangement, the refrigerant-rich solution was split into three streams that fed simultaneously the three generators. The authors reported that the triple-effect parallel-flow designs, similar to what they noticed in the case of double-effect cycles, always yielded a higher performance than the series-flow configurations. The performances reached at the specific thermal conditions $\left(T_{gen} = 260ºC;\ T_{evap} = 4.1ºC;\ T_{cond} = 32ºC\right)$ were $COP_{parallel} = 1.44$ vs. $COP_{series} = 1.29$. More elaborated triple-effect configurations were also reported to reach even higher values of the COP [18], $COP_{parallel} = 1.78$; $COP_{series} = 1.40$. Erickson et al. [19] studied a water/lithium bromide triple-effect absorption refrigerator. Their results showed that triple-effect absorption systems can attain a COP 50% over double-effect cycles, almost equal to 1.8. Kim et al. [20] theoretically analysed four configurations of compressor-assisted water/lithium bromide series-flow triple-effect absorption cooling cycles. The aim of their study was to reduce the temperature of the driving heat by 40ºC in order to avoid corrosion problems associated with generator temperatures over 180°C. In the considered

configurations the compressor was placed alternatively posterior to the high-pressure, the middle-pressure, the low-pressure generator or to the evaporator. The authors concluded that all four configurations were suitable as the COP was found to have increased from 1.54 in the case of the conventional triple-effect cycle to a COP of 1.70-1.74 for the newly proposed schemes. The work required of the compressor was about a 3–5% of the cooling capacity of equivalent mechanical energies. Using the software ABSIM [16-18], Kaita [21] investigated three configurations of the triple-effect water/lithium bromide absorption cooling cycle, namely parallel-flow, series-flow and reverse-flow. The author found that the parallel-flow configuration achieved the highest coefficient of performance (2.0); however the driving heat temperature exceeded 220°C. Gebreslassie et al. [22] estimated the coefficient of performance, the exergetic efficiency and the exergy destruction rate for half- to triple-effect water/lithium bromide absorption cooling cycles. The authors concluded that the COP increased significantly from the double to the triple-effect cycles and decreased gradually at high temperature heat sources. Similar trends were observed for the exergetic efficiency. Álvarez et al. [23] investigated a triple-effect absorption cooling cycle driven by high temperature heat sources (up to 260ºC). The cycle configuration consisted of a water/lithium bromide double-effect cycle coupled with a high pressure single-effect cycle in which an aqueous (lithium, potassium, sodium) nitrate solution was used as a working pair. The authors reported that the coefficient of performance was 1.73 at a heat source temperature of 250°C and a cooling water temperature of 30°C. Azhar et al. [24] carried out a performance and economic analysis of water/lithium triple-effect absorption cooling cycles. Depending on the configuration of the considered cycles, they found a COP in the range $(0.70 - 0.86)$ for single-effect, $(1.20 - 1.55)$ for double-effect and up to 2.16 for the optimized triple-effect designs. The results also showed that the operating cost of the double-effect cycle was about 68% of that of the single-effect cycle, the operating cost of the triple-effect cycle was 60 to 75% of that of the double-effect cycle and around 45% of that of the single-effect cycle. Shirazi et al. [25] investigated five configurations of solar absorption cooling and heating systems. The authors performed the analysis taking into account energetic, economic, and environmental aspects at different climate conditions. They reported that the COP of triple-effect cycle driven by solar collectors was between 1.61 to 1.72, depending on the location, and that the required temperature in the collector was about 210°C. They concluded that the extra capital cost compared to solar single-effect systems could be recovered in less than 10 years and that this configuration had the lowest carbon dioxide emissions of the systems

taken into consideration. Lizarte et al. [26] optimized the coefficient of performance of a parallel flow water/lithium bromide triple-effect absorption cooling system both under design and off-design conditions (for a variable-temperature heat source). For off-design conditions and at high generator temperatures ranging from 142°C to 227°C the optimal COP achieved was within the range of 1.05-2.13.

In conclusion of this literature overview, it can be stated that:

(i) The coefficient of performance of the conventional single and double-effect water/LiBr absorption chillers is rather low: 0.7 – 0.8 for the former and 1.0 – 1.2 for the latter.

(ii) The integration of ejectors into single and double-effect arrangements of absorption cooling systems can enhance their performance under specific working conditions.

(iii) The highest COPs are reached with triple-effect designs (up to 2) but, besides the growing complexity of these designs, temperatures over 180ºC are required for the heat source. At these working temperatures in the generator, the conventional working fluid water/LiBr suffers from serious problems of corrosion and thermal decomposition.

The objective of the present paper is to propose a novel ejector powered water/lithium bromide double-effect absorption/recompression refrigeration cycle driven by high temperature heat sources. The ejector is placed, as proposed in reference [11], in an external circuit to the absorption cycle, and is itself driven by a steam generator. The investigations, performed by numerical simulations, aim to assess the feasibility and the eventual improvement in performance of the proposed cycle configuration at temperatures of the driving steam ranging from 240ºC to 340ºC. The objective is to reach COP – values comparable to those of triple-effect cycles, maintaining the working temperature lower than 170ºC in the high pressure generator to overcome the corrosive effect and thermal instability of water/LiBr at high temperatures.

The operating principles of the absorption/recompression refrigeration cycle considered and the thermodynamic simulation methodology are described. The effect of the driving heat source temperature, the generator temperature and the ejector design on the cycle performance is analysed.

2. Configuration of the water/lithium bromide double-effect absorption/ recompression cycle

The ejector powered water/lithium bromide double-effect absorption/recompression cycle is shown schematically in Fig. 1. It comprises three fluid circuits: driving steam loop, refrigerant and solution circuits.

2.1. Steam circuit

A high temperature heat source is used in a steam generator to generate water vapour at high pressure (20). This is piped to the ejector primary nozzle, where an expansion takes place producing a high velocity jet and generating a partial vacuum in the mixing chamber of the ejector. A fraction (22) of the steam liberated in the high-pressure generator (HP-generator) is sucked off in this chamber and entrained by the primary flow. The mixed stream then passes through a supersonic-subsonic diffuser that compresses it to the pressure P_{23}. The exiting steam (23) condenses inside the tubing coil immersed in the salt solution of the HP-generator, liberating the heat needed for the desorption of water (17) from the aqueous solution. Part (27) of the condensate water from the heater coil (24) is pumped back into the steam generator via a water pump (W – PMP) and the rest (25) flows into the high-pressure condenser (HP-condenser).

The rest of the cycle is a conventional double-effect lithium bromide absorption cycle including the two remaining fluid circuits, solution and refrigerant loops.

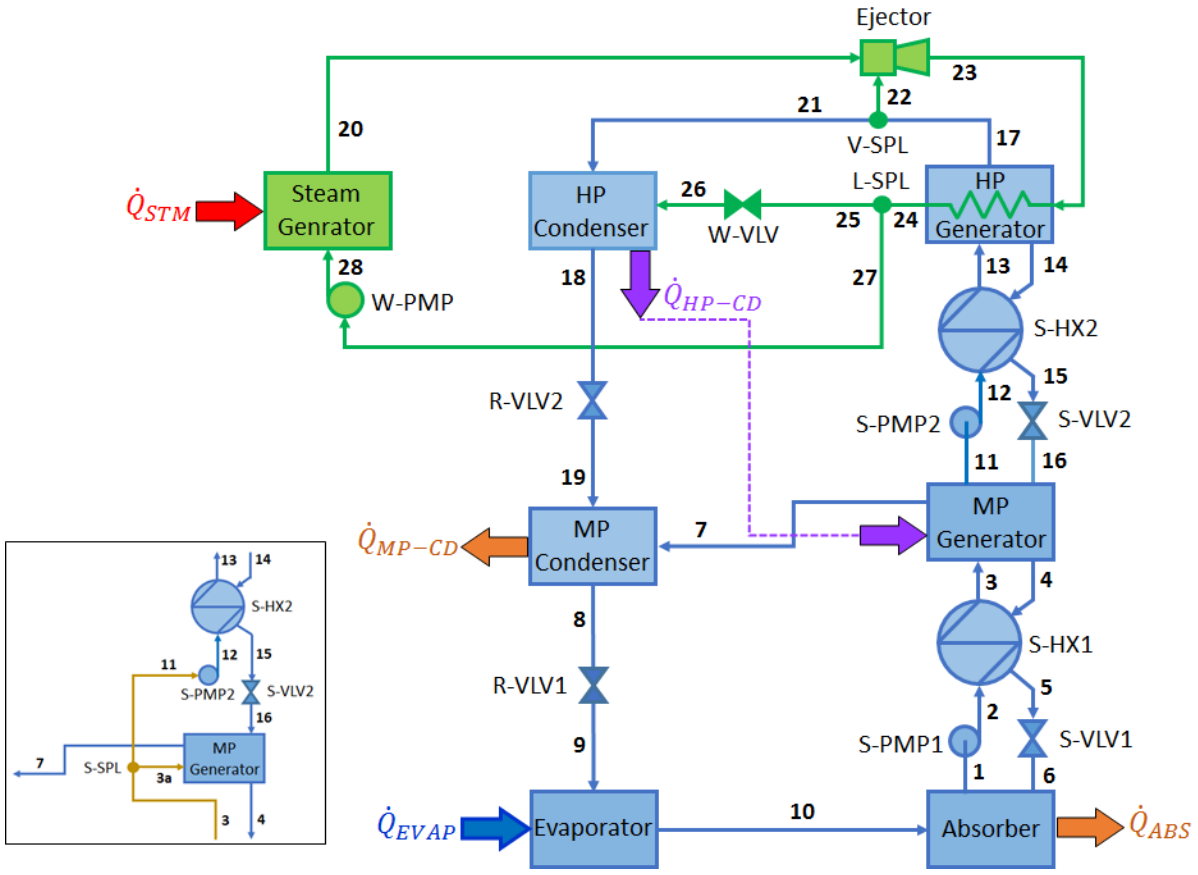

Figure 1. Schematics of the ejector powered double-effect absorption/recompression refrigeration cycle investigated

2.2.Refrigerant circuit

The HP-condenser is alimented by two streams. The first one (26) comes from the liquid water splitter (L – SPL) mounted at the exit of the HP-generator, after decompression to the appropriate pressure in the liquid expansion valve (W – VLV) takes place. The second stream is the rest (21) of the water vapour (17) liberated in the HP-generator. The released condensation heat $\dot{Q}_{HP-CD}$ is used to drive the water desorption in the intermediate-pressure generator (MP – generator). The formed condensate (18) passes through the valve R – VLV2 where its pressure is reduced to that of MP-condenser (19). The steam liberated in the MP-generator (7) also feeds this condenser. The exiting liquid water (8) undergoes a last adiabatic pressure reduction (R – VLV1), which causes a large decrease in temperature as a result of partial evaporation. It then flows (9) into the machine evaporator where it totally evaporates, making available the cooling capacity $\dot{Q}_{EVAP}$. Formed refrigerant vapours (10) are dissolved in the absorber by the salt-rich solution (6) returning from the generators. The heat released by this exothermic process $\dot{Q}_{ABS}$, like the condensation heat $\dot{Q}_{MP-CD}$ from the MP-condenser, is rejected to the cooling medium.

2.3. Solution circuit

The salt-weak (refrigerant-rich) solution leaving the absorber (1) is pumped (S – MP1) into the MP-generator pressure (2) and then preheated (3) in the solution heat exchanger (S – HX1). Particular to this double effect cycle is the fact that the MP-generator is fed by two solution streams. As illustrated in the box to the right of Fig.1, the splitter (S – SPL) divides the refrigerant-rich stream 3 into two parts: one part (3a), together with the partially cooled concentrated salt solution (16), feeds this generator, while the other part (11) flows further via the pump (S – MP2) and heat exchanger (S – HX2) to the HP-generator. The two mounted heat exchangers (S – HX1 and S – HX2) are used to recuperate heat from the salt-rich solutions (14 and 4) exiting the generators and to preheat the refrigerant-rich solution flowing counter-currently.

Two liquid expansion valves (S – VLV2 and S – VLV1) are mounted on the salt-rich solution line in order to reduce the pressure of the solution 14 gradually to that of the MP-generator (16) and finally to that of the absorber (6). The splitting ratio in the splitter (S – SPL) is set by the condition that the heat duty of the HP-condenser is large enough to produce as much vapour from the MP-desorber as is necessary to make the composition of the salt-rich solution (4) equal to that of the solution leaving the HP-generator (14), i.e.

$$x_4 = x_{14}$$

Fig. 2 presents the proposed cycle on the Dühring–diagram for a particular set of operating conditions. The solution circulation loop $(1-11-13-14-4-6)$ is similar to that of a conventional double effect absorption cycle: Water is taken up at the absorber $(6-1)$, released as vapor at the generators $(17 \text{ and } 7)$, and condensed at 18 and 8. In the considered cycle however, a fraction of the formed vapor 17 is compressed in the ejector and contributes to heat the solution 13 by condensation. Thus, heat otherwise rejected to the environment is recovered in order to improve the efficiency of the system. The ejector process is shown in Fig. 3 on $(P-h)-$chart. The external ejector loop processes are represented by the line $(20-\text{Nozzle exit}-23-24-28)$. In the mixing chamber, after expansion in the nozzle, stream 20 mixes with stream 22, and the resulting gas mixture is compressed to backpressure P23. The line through points $(18-19-8-9-10)$ represents a process series in the condensers and evaporator.

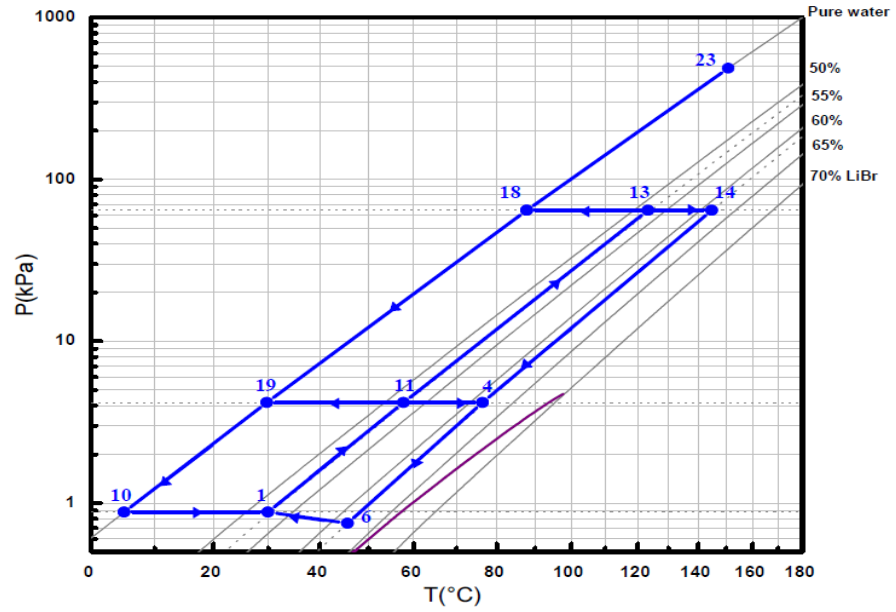

Figure 2. Dühring–diagram of the ejector powered double-effect absorption/recompression refrigeration cycle

3. Cycle simulation model

3.1 Mathematical modelling

In order to develop a simulation model for the configuration of the proposed absorption chiller, mass and energy balances are formulated for each machine component. Hypotheses and assumptions for the calculations are summarized in the following:

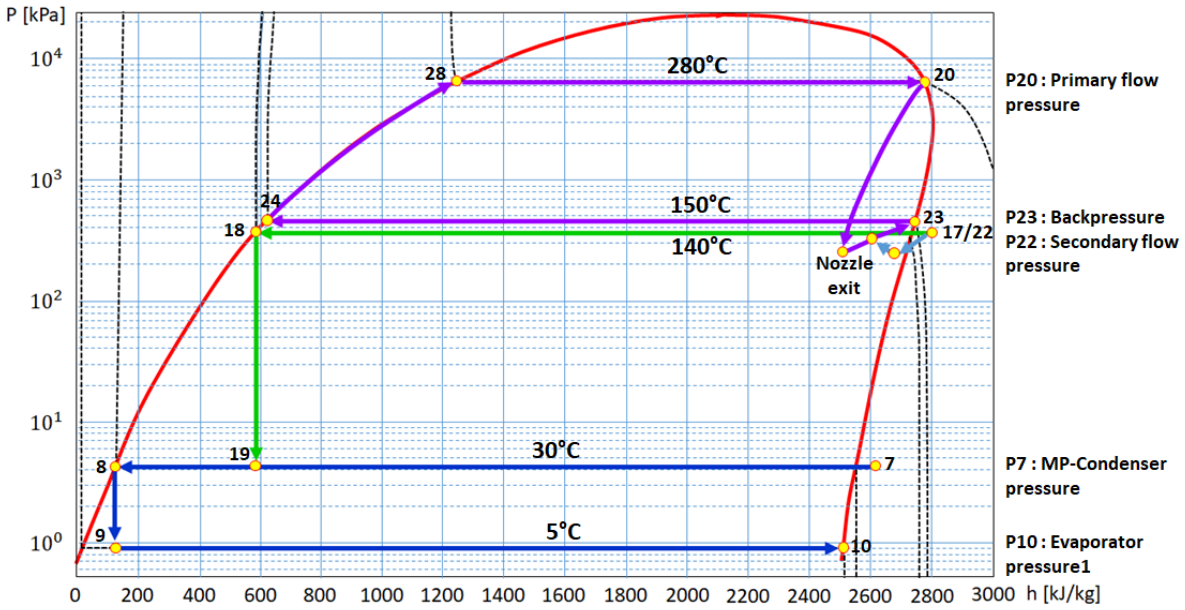

Figure 3. Ejector powered double-effect absorption/recompression refrigeration cycle on (P – h)–diagram of water

- Simulations and analyses are performed under steady state conditions.
- Heat losses to surroundings at generators, condensers, absorber and evaporator are negligible.
- Pressure losses in ducts and machine components are negligible.
- Refrigerant exiting condensers is in saturated liquid state.
- Refrigerant exiting evaporator is in saturated vapour state.
- Solution and refrigerant expansion valves are isenthalpic.
- Refrigerant vapour and liquid solution leaving generators are at same temperature.
- Liquid solutions leaving absorber and generators are saturated.
- Heat from HP-condenser covers intermediate generator heat needs with 5°C temperature pinch.
- Solution liquid compositions leaving generators are identical.
- Absorption and condensation temperatures are equal, $T_8 = T_1$.
- Evaporation temperature, T_{10}, is set to a fixed value.
- Effectiveness of heat exchangers is set to $\eta_{S-HX1} = \eta_{S-HX2} = 50\%$.
- Liquid pumping is isentropic, $\eta_{S-PMP1} = \eta_{S-PMP2} = \eta_{W-PMP} = 100\%$.

Neglecting kinetic and potential energy changes, the balance equations are as follows:

Total mass balance

$$\sum \dot{m}_{in} = \sum \dot{m}_{out} \quad (1)$$

Species mass balances

$$\sum (x_i \dot{m})_{in} = \sum (x_i \dot{m})_{out} \quad i = H_2O, LiBr \quad (2)$$

Energy balance

$$\sum (\dot{m}h)_{in} - \sum (\dot{m}h)_{out} + \dot{W} + \dot{Q} = 0 \quad (3)$$

$\dot{Q}$ and $\dot{W}$ are heat and work transfer rates, respectively.

The system coefficient of performance COP, is per definition:

$$COP_{ED} = \frac{\dot{Q}_{EVAP}}{\dot{Q}_{STM} + \sum \dot{W}_P} \approx \frac{\dot{Q}_{EVAP}}{\dot{Q}_{STM}} \quad (4)$$

As an illustration of the modelling procedure, the particular case of the steam generator-loop is treated.

Steam generator loop model

The generator loop encompasses the machine components steam generator, ejector, high-pressure desorber, expansion valve, stream-splitter, and water pump.

a. High-pressure desorber

- Total mass balance

  $\dot{m}_{13} + \dot{m}_{23} = \dot{m}_{14} + \dot{m}_{17} + \dot{m}_{24}$ (5)

  Since $\dot{m}_{23} = \dot{m}_{24}$, this equation reduces to

  $\dot{m}_{13} = \dot{m}_{14} + \dot{m}_{17}$ (6)

- LiBr mass balance

  $\dot{m}_{13} x_{13} = \dot{m}_{14} x_{14}$ (7)

  Combining both the latter equations leads to

  $\dot{m}_{14} = \dot{m}_{17} \frac{x_{13}}{x_{14} - x_{13}} \quad \dot{m}_{13} = \dot{m}_{17} \frac{x_{14}}{x_{14} - x_{13}}$ (8)

- Energy balance

  $\dot{m}_{23}(h_{23} - h_{24}) + \dot{m}_{17} \frac{x_{14}}{x_{14} - x_{13}} h_{13} = \dot{m}_{17} h_{17} + \dot{m}_{17} \frac{x_{13}}{x_{14} - x_{13}} h_{14}$ (9)

b. Ejector

- The entrained vapour flow rate $\dot{m}_{22} (= \dot{m}_{25} = \dot{m}_{26})$ is written as

  $\dot{m}_{22} = \omega \, \dot{m}_{20}$ (10)

  where ω is the ejector entrainment ratio and $\dot{m}_{20}$, the motive steam flow rate. The mixed gas flow rate $\dot{m}_{23} (= \dot{m}_{24})$ is then:

  $\dot{m}_{23} = (1 + \omega)\dot{m}_{20}$ (11)

  Combining with the energy balance of the high-pressure generator leads finally to

  $\dot{m}_{20} = \dot{m}_{17} \frac{(h_{17} - h_{13}) + F_2(h_{14} - h_{13})}{(1 + \omega)(h_{23} - h_{24})}$ (12)

  where $F_2 = \frac{\dot{m}_{14}}{\dot{m}_{17}} = \frac{x_{13}}{x_{14} - x_{13}}$ is the circulation factor in the new cycle configuration.

- Energy balance

$$h_{20} + \omega h_{22} = (1+\omega) h_{23} \Longrightarrow h_{23} = \frac{h_{20}+\omega h_{22}}{1+\omega} \quad (13)$$

c. Water pump

- Mass balance

$$\dot{m}_{28} = \dot{m}_{27} = \dot{m}_{20} \quad (14)$$

- Energy balance

$$\dot{m}_{20} h_{27} + \dot{W}_{w-PMP} = \dot{m}_{20} h_{28} \quad (15)$$

with

$$\dot{W}_{w-PMP} = \dot{m}_{20} \frac{P_{28} - P_{27}}{\rho_{27}} \quad (16)$$

d. Steam generator

- Mass balance

$$\dot{m}_{20} = \dot{m}_{28} \quad (17)$$

- Energy balance, with Q_{STMG} the driving heat supplied to the chiller at the steam generator

$$Q_{STMG} = \dot{m}_{20} (h_{20} - h_{24}) \quad (18)$$

e. Expansion valve

- Mass balance

$$\dot{m}_{25} = \dot{m}_{26} (= \dot{m}_{22}) \quad (19)$$

- Energy balance

$$h_{25} = h_{26} (= h_{27} = h_{24}) \quad (20)$$

f. Further, setting T_{24} for the temperature of condensing steam in the heating coil and P_{17} for the secondary flow pressure (high-pressure in the HP-generator), the properties of the salt-rich solution and the water-vapour exiting this generator can be evaluated based on the equilibrium data of the water-lithium bromide system:

$T_{14} = T_{24} - \Delta T_G$ (ΔT_G is set to 5K in simulations) ;

$x_{14} = x_{sat}(T_{14}, P_{17})$; $h_{14} = h_{sat-liq}(T_{14}, x_{14})$; $h_{17} = h_{sat-vap}(T_{14}, P_{17})$

The properties of saturated pure liquid water exiting the heating coil are evaluated using steam tables

$P_{24} = P_{sat-steam}(T_{24})$; $h_{24} = h_{sat-liq-water}(T_{24})$

Similarly for the properties of the saturated steam leaving the steam generator at fixed temperature T_{20}

$P_{20} = P_{sat-steam}(T_{20})$; $h_{20} = h_{sat-steam}(T_{20})$

3.2 Theoretical cooling efficiency

The heat released by the condensation of the mixed vapour stream $\dot{m}_{23}$ in the high-pressure generator can be evaluated using the energy balance of this machine component (Eq. 8)

$$\dot{m}_{20} = \dot{m}_{17}\frac{(h_{17} - h_{13}) + F_2(h_{14} - h_{13})}{(1+\omega)(h_{23} - h_{24})} \tag{21}$$

This equation gives the relation between the motive steam flow-rate $\dot{m}_{20}$, the desorbed refrigerant flowrate $\dot{m}_{17}$, the entrainment ratio ω, the thermodynamic state of the salt weak and strong solutions, (h_{13}, h_{14}), the circulation ratio F_2 and the specific condensation enthalpy $(h_{23} - h_{24})$.

The useful cold $\dot{Q}_{EVAP}$ is produced by the evaporation of the refrigerant in the machine evaporator,

$$\dot{Q}_{EVAP} = (\dot{m}_{17} + \dot{m}_7)(h_{10} - h_9) \tag{22}$$

Neglecting the energy supplied to the three pumps, it follows that for the coefficient of performance of the proposed cycle, COP_{ER}:

$$COP_{ER} = \frac{\dot{Q}_{EVAP}}{\dot{Q}_{STM}} = \frac{(\dot{m}_{17} + \dot{m}_7)(h_{10} - h_9)}{\dot{m}_{20}(h_{20} - h_{28})} \tag{23}$$

$$COP_{ER} = (1+\omega)\frac{(h_{10} - h_9)(h_{23} - h_{24})}{\big((h_{17} - h_{13}) + F_2(h_{14} - h_{13})\big)(h_{20} - h_{28})} + (1+\omega)\left(\frac{\dot{m}_7}{\dot{m}_{17}}\right)\frac{(h_{10} - h_9)(h_{23} - h_{24})}{\big((h_{17} - h_{13}) + F_2(h_{14} - h_{13})\big)(h_{20} - h_{28})} \tag{24}$$

Setting α for the ratio of the refrigerant amount generated in the intermediate-pressure and high-pressure generators, $\alpha = \frac{\dot{m}_7}{\dot{m}_{17}}$, the final expression for the coefficient of performance becomes

$$COP_{ER} = \frac{\dot{Q}_{EVAP}}{\dot{Q}_{STM}} = \left[(\alpha+1)\frac{(h_{10} - h_9)}{(h_{17} - h_{13}) + F_2(h_{14} - h_{13})}\right]\left[(1+\omega)\frac{(h_{23} - h_{24})}{(h_{20} - h_{28})}\right] \tag{25}$$

The expression of COP_{ER} is thus the product of two terms. The former on the left side of equation (25) represents the theoretical expression of the performance of a conventional double-effect cycle and the latter, an enhancement factor. It describes the performance

improvement as a result of the use of the steam ejector. Therefore, the considered cycle is virtually a double effect cycle with an enhanced performance due to the steam ejector

$$\mathrm{COP_{ER}} = \frac{\dot{Q}_{\mathrm{EVAP}}}{\dot{Q}_{\mathrm{STM}}} = \epsilon\, \mathrm{COP_{conv}} \tag{26}$$

The ratio $\frac{(h_{23}-h_{24})}{(h_{20}-h_{28})}$ in the enhancement factor indicates the fraction of the energy supplied to the motive stream $(h_{20} - h_{28})$ used to heat the salt solution in the HP-generator. Because $h_{28} \simeq h_{24}$, it follows that:

$$\frac{(h_{23} - h_{24})}{(h_{20} - h_{28})} \simeq \frac{(h_{23} - h_{24})}{(h_{20} - h_{24})} = \frac{(h_{20} - h_{24})}{(h_{20} - h_{24})} - \frac{(h_{20} - h_{23})}{(h_{20} - h_{24})} = 1 - \frac{(h_{20} - h_{23})}{(h_{20} - h_{24})} \tag{27}$$

$\frac{(h_{20}-h_{23})}{(h_{20}-h_{24})}$ is the fraction of supplied heat $(h_{20} - h_{24})$ used to entrain the vapour by the ejector from the solution chamber into the coil. So theoretically to get the best energy performance, one has to optimize the enhancement factor ϵ by minimizing the ratio $\frac{(h_{20}-h_{23})}{(h_{20}-h_{24})}$ and maximizing the entrainment factor ω. This result emphasizes the huge influence of the ejector operation on the performance of the novel cycle.

4. Model validation

Using the software Engineering Equation Solver, EES [27], a computer code simulating the steady-state behavior of the refrigerator and an analysis of its performances under various operating conditions was developed. The thermo-physical properties of the working fluid system H_2O/LiBr are available as internal functions in the software library.

The simulation program consists of two subprograms corresponding to the actual refrigerator configuration: a subprogram for the water-lithium bromide circuit and another for the driving steam circuit with the ejector as the main component.

Before running the simulations for the ejector powered double-effect absorption/recompression cycle, the simulation program was first tested and validated by comparing the calculated results with the literature data whenever available. For the validation, three tests were performed. First, the ejector subprogram was validated. Then, the simulation model was tested for an ejector driven single-effect absorption cycle. Finally, the main program was validated for a conventional double-effect absorption chiller without ejector.

4.1 Ejector model validation

Detailed mathematical formulations of the ejector 1D flow model are described in the Appendix. Given the operating conditions (primary, secondary and backpressure) as well as the geometry of the ejector, an iteration procedure was applied to determine the entrainment ratio ω. For the validation of the ejector model experimental bibliographical data were used [28, 29]. Three adjustable parameters were introduced to account for the irreversibility of gas expansion in nozzle (η_n) and diffuser (η_d), and for mixing of primary and secondary streams (η_m). Eleven ejectors with an ejector area ratio $\left(\frac{A_c}{A_t}\right)$ ranging from 6.44 to 10.64 and a nozzle throat diameter between 2.62 mm and 2.82 mm were tested using $R141b$ as a working fluid. As illustration of the obtained results, Figs. 4a and 4b show that with the set of values $(\eta_n = 0.95, \eta_d = 0.85, \eta_m = 0.88)$, the experimental data reported in reference [29] were fairly reproduced. The difference observed in Fig. *4b* is probably due to the parameter η_m set in our calculations as constant while in reference [29] its value was varied with the ejector area ratio $\left(\frac{A_c}{A_t}\right)$.

The average absolute deviation between experimental and calculated entrainment ratio is 8%. This value is acceptable considering the large number of algebraic equations in the theoretical ejector model and the adoption of perfect gas assumption in these equations.

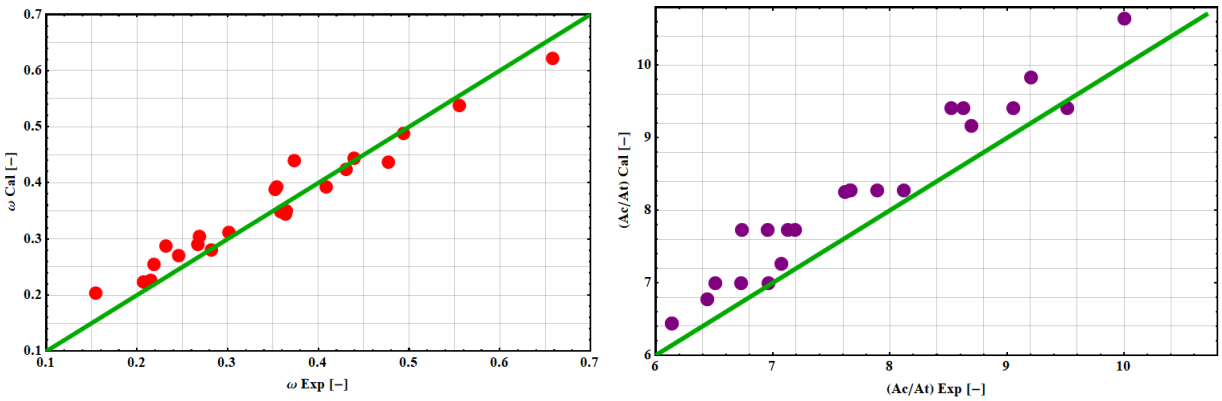

(*a*) (*b*)

Figure 4. Validation of the ejector model based on experimental data of reference [28]

4.2 Validation using the ejector powered single-effect absorption/recompression cycle

To our knowledge, only one reference [12] reports on experimental and theoretical investigations of re-compression cycles with an ejector in the external loop, which however deals solely with single effect configurations. The data presented in this paper are used for the partial validation of our program after modification to accommodate the configuration considered.

The simulations were performed for similar operating conditions: equal absorption and condensation temperatures ($T_{cond} = T_{abs} = 30ºC$), evaporator temperature ($T_{evap} = 5ºC$), driving steam temperature of 198.3°C (corresponding to a saturation pressure of 15 bar), 54% salt concentration in liquid solution leaving the absorber, 50 mbar secondary pressure, and cooling capacity of 5 kW.

Fig. 5 shows a comparison of predicted COP with the experimental data reported in reference [12]. As can be noticed, the concordance is good, with a maximum deviation of 4% between both sets of data. In view of the scattering of the experimental data and the simplifying assumptions in the ejector model, the deviation can be considered acceptable. Further, it is worth note that the COP of this single-effect absorption/recompression cycle is almost 1,

which is higher than the values (~0.7) usually achieved with conventional water/lithium bromide single-effect absorption cycles.

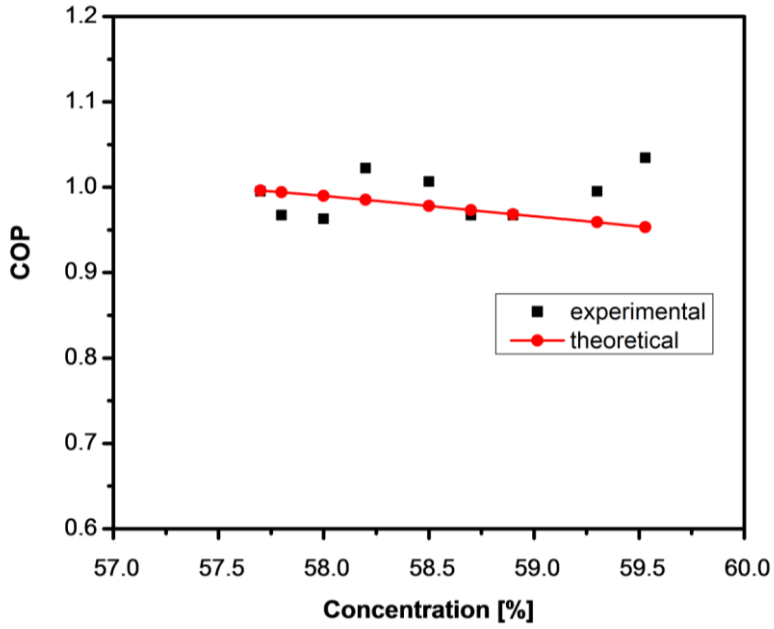

Figure 5. Model predicted COP *vs*. LiBr-concentration in the generator in comparison with experimental data from reference [12]

4.3 Validation using a double-effect absorption refrigeration cycle without an ejector

The third test of our program was based on the simulation results reported by Somers et al. [30], obtained using an ASPEN PLUS model for a double-effect absorption chiller. The simulations were performed under following operating conditions: Evaporator temperature, 5.1°C; condenser temperature, 29.7°C; absorber temperature, 29.9°C; heat exchanger effectiveness, 0.5 and flow rate of refrigerant-rich solution leaving the absorber, 1kg/s. Table 1 shows a detailed comparison of our simulation results with the data reported in reference [29]. As can be noticed, the obtained results are well in agreement with the published data. Calculated temperatures are almost identical, with a maximum deviation of 0.4%. Pressure deviations for low, medium and high pressure are 0.3%, 0.1%, and 4%, respectively. The gap in LiBr-concentration is approximately 0.6%. Finally the absolute average deviation in flow rate is 0.9%, an acceptable value as the flow rate is calculated according to mass and energy balances, so it accumulates all the previous deviations. In conclusion, this subprogram of our simulation tool can be considered validated as the calculated cycle data are well in agreement with those reported in reference [30].

Table 1. Comparison of results calculated with data from reference [30]

Point	T (°C)		P (kPa)		$\dot{m}$ (kg/s)		X (% LiBr)	
	ref. [30]	Present work	ref. [30]	Present work	ref. [30]	Present work	ref. [30]	Present work
1	29.9	29.9	0.881	0.88	1	1.000	52.7	52.5
2	29.9	29.9	4.178	4.173	1	1.000	52.7	52.5
3	46.9	47.6	4.178	4.173	1	1.000	52.7	52.5
4	74.9	75.8	4.178	4.173	0.856	0.857	61.6	61.2
5	52.4	52.9	4.178	4.173	0.856	0.857	61.6	61.2
6	45.5	47.5	0.881	0.88	0.856	0.857	61.6	61.2
7	57.7	57.8	4.178	4.173	0.066	0.064	0	0
8	29.7	29.7	4.178	4.173	0.144	0.143	0	0
9	5.1	5.1	0.881	0.88	0.144	0.143	0	0
10	5.1	5.1	0.881	0.88	0.144	0.143	0	0
11	57.7	57.8	4.178	4.173	0.541	0.549	52.7	52.5
12	57.8	57.8	64.37	66.73	0.541	0.549	52.7	52.5
13	91.1	91.6	64.37	66.73	0.541	0.549	52.7	52.5
14	144.8	144.8	64.37	66.73	0.463	0.471	61.6	61.2
15	101.3	101.3	64.37	66.73	0.463	0.471	61.6	61.2
16	77.1	78	4.178	4.173	0.463	0.471	61.6	61.2
17	123.3	124.7	64.37	66.73	0.078	0.078	0	0
18	87.8	88.7	64.37	66.73	0.078	0.078	0	0
19	29.7	29.7	4.178	4.173	0.078	0.078	0	0

5. Thermodynamic analysis of the ejector driven double-effect cycle: simulation results and discussion

The first step in our investigations of the proposed cycle was an extension of the last test. For similar operating conditions, a steam driven ejector was integrated in the double-effect absorption/recompression cycle (Fig. 1) and the effect of the primary flow pressure P_{20}, fixed by the generated steam temperature T_{20}, was analysed. Specific conditions for this base case study are given in Table 2. The simulation results are depicted in Fig. 6 representing the COP evolution with HP-generator temperature T_{14} for various driving steam temperatures T_{20} and in comparison with the COP behaviour of a conventional double-effect absorption refrigeration cycle.

Table 2. Base case study conditions

T_{20}[°C]	T_{14}[°C]	Nozzle area ratio $\left(\frac{A_n}{A_t}\right)$
200	[103 – 127]	5
240	[103 – 145]	8
280	[103 – 151]	12
320	[103 – 155]	18
340	[103 – 158]	20

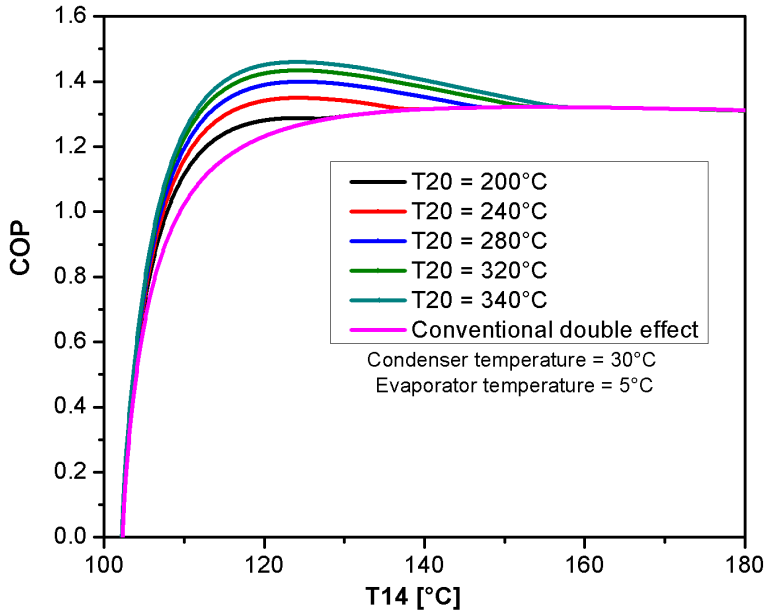

Figure 6. COP *vs.* HP–generator temperature T_{14} for various driving steam temperatures T_{20}

In view of these results we notice that:

- For the conventional double-effect cycle, the highest $\mathrm{COP} = 1.32$ is reached by an HP-generator temperature of 150°C.
- For ejector driving steam temperatures of 200°C and larger, the COP increases, reaches a maximum and decreases progressively to join the COP −curve of the double-effect absorption cycle.
- The COP −maximum occurs at HP−generator temperatures in the range of 120°C–125°C, thus it is lower by 20°C to 25°C than that of the maximum COP for the conventional double-effect absorption cycle.
- The maximum COP is higher as the driving steam temperature increases: 1.38 for $T_{20} = 240$ºC, 1.40 for $T_{20} = 280$ºC, 1.43 for $T_{20} = 320$ºC and 1.44 for $T_{20} = 340$ºC. The calculations show that the enhancement factor ϵ, and consequently the COP, increases

with increasing T_{20} and HP–generator temperature: from 1.0 (no enhancement) to 1.24 for $T_{14} = 105ºC$ and from 1.34 to 1.7 for $T_{14} = 135ºC$, i.e., $\Delta\epsilon = 0.24$ for the lower HP–generator temperature and $\Delta\epsilon = 0.36$ for the higher temperature.

In conclusion for these base-case simulations, we note that for the cycle considered, the predicted COP generally increases with the heat source temperature. So driving steam temperatures should be kept as high as possible to achieve larger enhancement factors and higher performances. Similar effects will be observed in the results of the following investigations.

The object of the following simulations was to carry out a sensitivity analysis of the proposed chiller configuration with respect to the variations in thermal conditions of the chilled water (cooling effect), the cooling medium used to dissipate the heat released in the absorber and MP−condenser and to the operating conditions of the ejector. Chilled water was set either at 7°C or 15°C, corresponding to the evaporator temperatures of 4°C and 12°C, respectively. The MP−condenser and absorber were supposedly working alternatively at 35°C and 40°C. Table 3 summarizes these conditions. Table 4 gives the ejector geometry and the primary stream conditions considered for the various cases. The nozzle area ratios were selected so that for a fixed steam generator temperature, *i.e.* primary flow pressure P_{20}, the entrainment ratio ω was at or near maximum. Further, it was tested so that in each case the cycle representation on the Dühring−diagram was far from the crystallization line, so avoiding any risk of crystallization.

Table 3. Operating conditions investigated

Case #	Thermal conditions	Pinch at HX-inlet, ΔT_{Pinch}	$\Delta T = T_{out} - T_{in}$
1	$T_8 = T_1 = 35ºC$ $T_{10} = 4ºC$	$\Delta T_{Pinch,\ evap} = 3ºC$ $\Delta T_{Pinch,\ abs\ (cond)} = 3ºC$	$\Delta T_{Cooling\ Medium} = 5ºC$ $\Delta T_{Chilled\ Water} = -5ºC$
2	$T_8 = T_1 = 40ºC$ $T_{10} = 4ºC$	$\Delta T_{Pinch,\ evap} = 3ºC$ $\Delta T_{Pinch,\ abs\ (cond)} = 3ºC$	$\Delta T_{Cooling\ Medium} = 5ºC$ $\Delta T_{Chilled\ Water} = -5ºC$
3	$T_8 = T_1 = 35ºC$ $T_{10} = 12ºC$	$\Delta T_{Pinch,\ evap} = 3ºC$ $\Delta T_{Pinch,\ abs\ (cond)} = 3ºC$	$\Delta T_{Cooling\ Medium} = 5ºC$ $\Delta T_{Chilled\ Water} = -5ºC$
4	$T_8 = T_1 = 40ºC$ $T_{10} = 12ºC$	$\Delta T_{Pinch,\ evap} = 3ºC$ $\Delta T_{Pinch,\ abs\ (cond)} = 3ºC$	$\Delta T_{Cooling\ Medium} = 5ºC$ $\Delta T_{Chilled\ Water} = -5ºC$

It should be noted further that the simulations are performed by assuming a value of 0.85 for nozzle and diffuser efficiencies, ($\eta_n = \eta_d = 0.85$). Primary and secondary mixing is supposed to provoke no notable irreversibility ($\eta_d = 1$).

Table 4. Nozzle area ratio and primary flow temperature for cases dealt with

	Nozzle area ratio $\left(\frac{A_n}{A_t}\right)$			
Primary flow temperature, T_{20} (Saturated steam)	Case #1	Case #3	Case #2	Case #4
200ºC	4	5	4	4
240°C	7	8	5	6
280°C	9	11	7	8
320°C	13	17	10	12

5.1. Effect of evaporator and condenser/absorber temperatures

The results of the simulations of the cases #1 to #4 are depicted graphically in Figs. 7. Table 6 summarizes the most important results.

The COP of the conventional double-effect configuration expectedly increases with an increase in HP–generator temperature T_{14}, it reaches a maximum and then decreases slowly. The maximum performance depends also on the evaporator and condenser/absorber

temperature, T_{10} and T_8 (or T_1) respectively. The lowest COP is seen in the cycle with the lowest evaporator temperature ($T_{10} = 4ºC$) and highest condenser and absorber temperature ($T_1 = 40ºC$): $COP = 1.17$ at $T_{14} = 200ºC$. Conversely, a $COP = 1.35$ produced by an HP–generator temperature $T_{14} = 155ºC$ is obtained in a thermodynamically favourable case (lower absorber/condenser temperature, $T_1 = 30ºC$, and higher evaporator temperature, $T_{10} = 12ºC$. Following are some specific remarks.

- As observed earlier in the discussion of Fig. 6, the maximum COP is higher as the driving steam temperature increases. In fact, for the lowest steam temperature, $T_{20} = 200ºC$, no or insignificant effect is noticed in the case studies #1, #2 and #4, as the COP −curves for ejector driven and conventional cycles cover each other. This is also true for steam temperature $T_{20} = 240ºC$ in case #2.
- For cases #1 and #2, the enhancement effect of the ejector recompression on the maximum COP is insignificant; however, this maximum is now reached at lower HP–generator temperature (by 25°C less).
- The maximum enhancement of the COP is observed in case #3 (35°C at the absorber/condenser and 12°C at the evaporator). Here a maximum COP of 1.57 is reached at $T_{14} = 120ºC$. The performance improvement is lower in the case of a higher cooling temperature (case #4). For the highest steam temperature, a COP of 1.35 is reached at $T_{14} = 145ºC$.
- The effect of the ejector recompression is limited to a specific HP–generator temperature range ΔT_{14} depending on the driving steam temperature. For higher T_{20} the range ΔT_{14} is more extended. The last column of Table 6 gives ΔT_{14} for cases #1 to #4 at the highest driving steam temperature $T_{20} = 320ºC$. It is noteworthy also that this range is dependent on the operation conditions and increases with increasing COP maximum.

On concluding this part of the investigations, it is noted that the ejector recompression technique affects the performance of the double-effect absorption cycle in two aspects: improvement of the COP as in the cases #3 and #4 and the shift of maximum COP at lower HP–generator temperatures in all the cases considered.

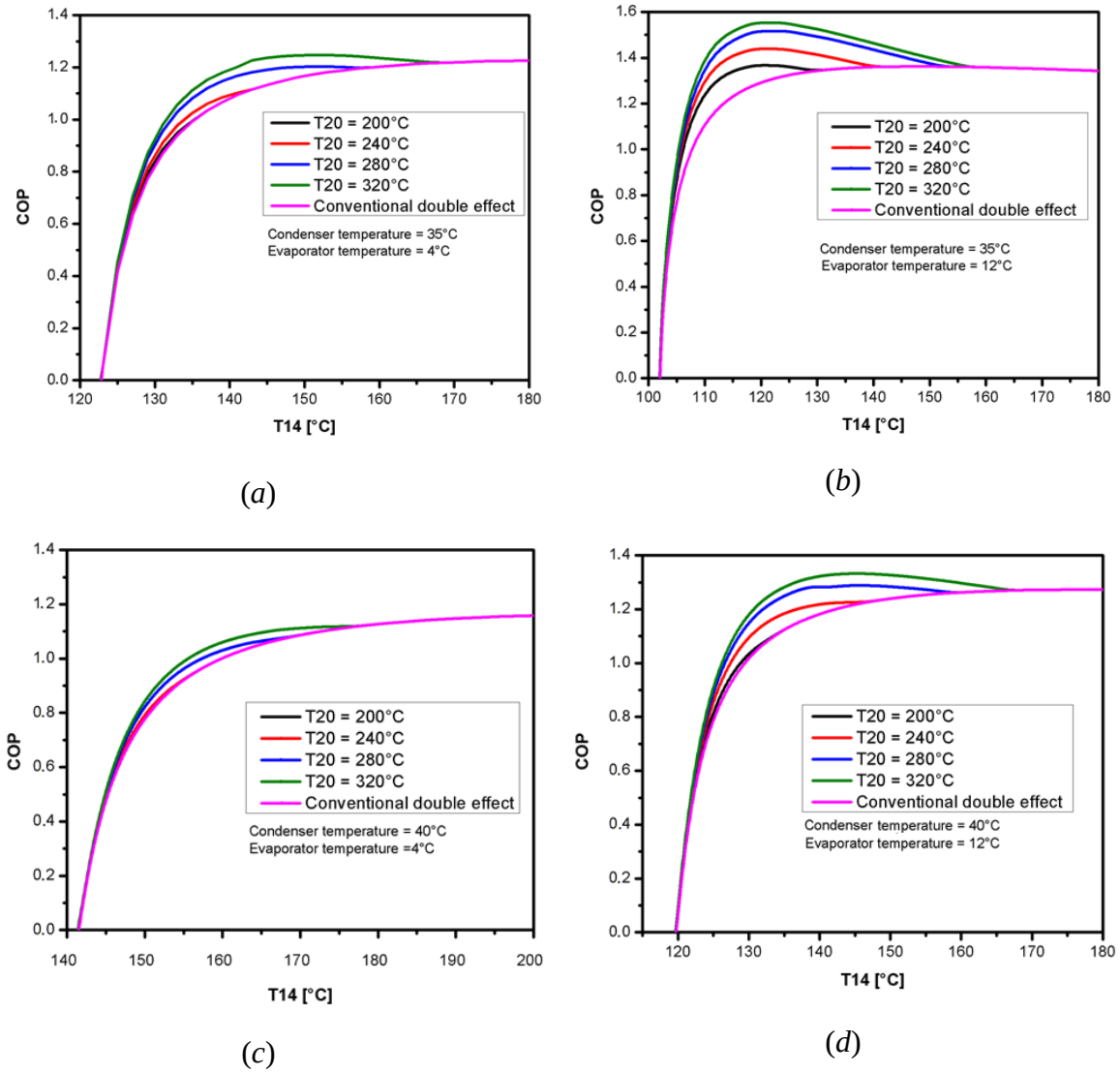

Figure 7. COP *vs*. HP–generator temperature T_{14} for the cases #1 (a), #3 (b), #2 (c) and #4 (d) and various driving steam temperatures T_{20}

5.2. Effect of ejector operation

We now focus attention on the ejector operation to interpret some of the simulation results previously presented. As an illustration, Figs. 8(*a*) and 8(*b*) depict the evolution of the entrainment ratio for cases #1 and #2 with HP–generator temperature T_{14} for various primary flow temperatures T_{20}. One notices that ω decreases monotonously, quasi-linearly, with increasing T_{14} and vanishes at a certain temperature. The same behaviour is observed when varying the T_{20}. However, when the primary flow temperature is increased, the ω *vs*. T_{14} line is shifted up to higher values of the entrainment ratio, and the limit temperature T_{14} is pushed farther away. For case #1 the maximum value of ω (0.5) is reached at the lowest possible temperature $T_{14} = 120ºC$ and the highest considered $T_{20} = 320ºC$. For the

thermodynamically less favorable case #2 (Fig. 8*b*), a maximum $\omega = 0.37$ is obtained at $T_{14} = 140ºC$ and the highest T_{20}. Further the range of T_{14} in Figs. 7 (and Table 5), where an enhancement of the COP is observed corresponds to the feasible, non-vanishing range of ω in Figs. 8(*a*) and 8(*b*).

Table 5. Summary of simulation results

Case #	Conventional double-effect	Ejector recompression double-effect $T_{20} = 320ºC$	Temperature range for COP–Enhancement
1: $T_8 = T_1 = 35ºC$ $T_{10} = 4^\circ C$	Max COP = 1.25 @ $T_{14} = 175ºC$	Max COP = 1.25 @ $T_{14} = 150ºC$	$\Delta T_{14} \approx 45ºC$
2: $T_8 = T_1 = 40ºC$ $T_{10} = 4ºC$	Max COP = 1.17 @ $T_{14} = 200ºC$	Max COP = 1.11 @ $T_{14} = 175ºC$	$\Delta T_{14} \approx 35ºC$
3: $T_8 = T_1 = 35ºC$ $T_{10} = 12^\circ C$	Max COP = 1.35 @ $T_{14} = 155ºC$	Max COP = 1.57 @ $T_{14} = 120ºC$	$\Delta T_{14} \approx 55ºC$
4: $T_8 = T_1 = 40ºC$ $T_{10} = 12ºC$	Max COP = 1.27 @ $T_{14} = 170ºC$	Max COP = 1.35 @ $T_{14} = 145ºC$	$\Delta T_{14} \approx 48ºC$

The behaviour of ω *vs.* backpressure depicted in Figs. 8(*c*) and (*d*) matches up with its evolution *vs.* T_{14}, since the flow 23 exiting the ejector (Fig. 1) constitutes the heat source for the HP–generator. A rise (or drop) of backpressure P_{23} –and consequently of T_{23}– results in an increase (or decrease) of the HP–generator temperature T_{14}. In fact, the secondary flow pressure and salt solution in the HP–generator are monotonously increasing functions of the backpressure for fixed primary flow conditions and constant absorber/condenser temperature. The ejector model presented in the Appendix will help interpret the numerical simulation results and apprehend the beneficial effects –and limits–of the integration of ejectors into an absorption chiller. According to this model, the entrainment ratio depends on nozzle area ratio, primary flow and secondary flow stagnant properties, and backpressure, *i.e.*

$$\omega = f\left(\frac{A_n}{A_t}, P_{20}, T_{20}, P_{22}, T_{22}, P_{23}\right) \tag{28}$$

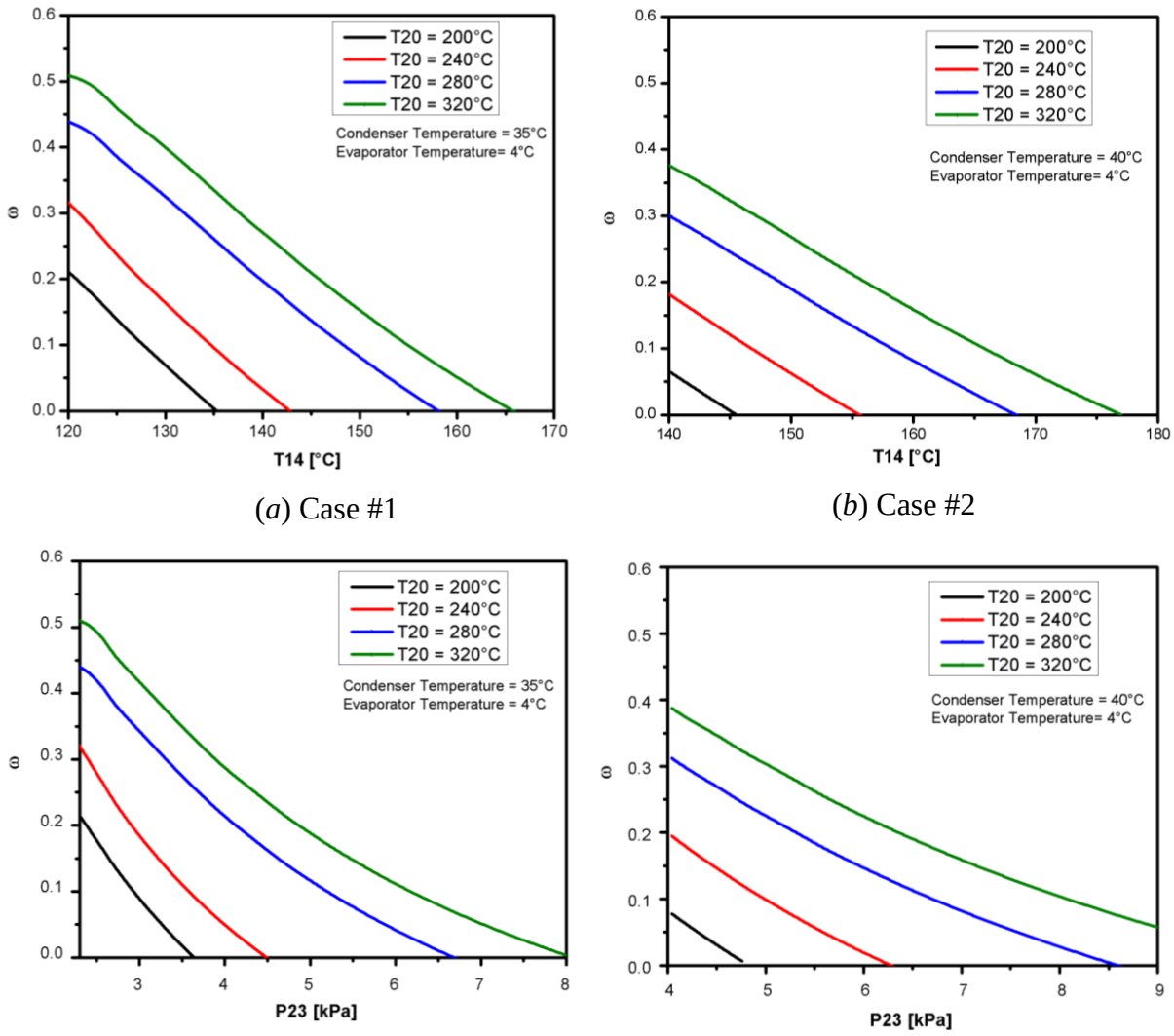

Figure 8. Effect of HP–generator temperature T_{14} (*a* & *b*) and backpressure (*c* & *d*) on entrainment ratio ω for cases #1 and #2

However, and as mentioned earlier, in an ejector driven chiller the secondary flow properties depend on the processes taking place in the HP–generator. These are determined by the evaporator and absorber/condenser temperatures (salt concentration of incoming solution) as well as by the temperature of the heating coil, *i.e.*, by the backpressure properties. For fixed driving flow conditions and absorber/condenser temperature, the entrainment ratio thus depends solely on nozzle geometry (A_n/A_t) and back pressure P_{23}, $\omega = f(A_n/A_t, P_{23})$. As an illustration of this dependency, Fig. 9(*a*) depicts the evolution of ω with nozzle area ratio and backpressure for case #3 with a primary flow temperature $T_{20} = 240ºC$ ($P_{20} = 33.4$ bar). It shows that for fixed values of P_{23} the entrainment ratio first grows with increasing (A_n/A_t), reaches a maximum, then decreases and finally vanishes. Conversely, for a constant nozzle

area ratio, ω increases with falling backpressure, passes through a maximum and decreases to zero. Fig. 9(*a*) reveals also that the extent of the feasible variation range for both variables reduces continuously for higher entrainment ratios, culminating in one single point. Further, larger values of ω are obtained for lower values of the variables (A_n/A_t) and P_{23}. The intersection of a horizontal plane with the 3D-surface in Fig. 9(*a*) (illustrated in light green for $\omega = 0.3$) is a curve representing the set of variable couples generating the same entrainment ratio. The projection of such intersection lines on the basis horizontal plane constitutes a so-called contour plot sketch of the 3D–surface, depicted in Fig. 9(*b*).

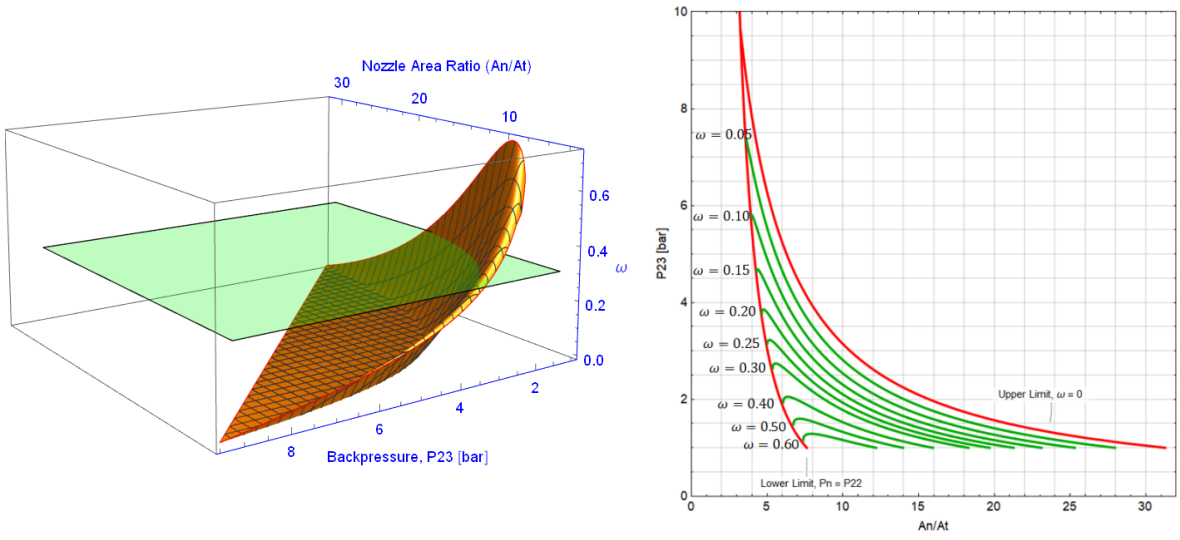

(*a*) (*b*)

Figure 9. (*a*) 3D-representation of entrainment ratio *vs*. nozzle area ratio and backpressure for case #3 at driving steam temperature $T_{20} = 240ºC$ ($P_{20} = 33.4$ bar) ; (*b*) Contour plot representation of the same

The 3D−surface $\omega = f(A_n/A_t, P_{23})$ as well as its contour plot representation are bounded. In Fig. 9(*a*) the feasible ω region is limited by two curves plotted in red corresponding to $\omega = 0$. Beyond these limits the ejector is in off-design conditions and will not work.

Consider first the limit of the feasibility domain for lower nozzle area ratios ("Lower Limit" curve in Fig. 9(*b*)). This curve sets a geometrical lower limit to the nozzle design. In fact,

with decreasing nozzle area ratio (A_i/A_t), the nozzle exit pressure P_n expectedly rises and comes closer to the secondary flow pressure P_{22}. The suction of the secondary flow into the mixing chamber, driven by the pressure difference ($P_{22} - P_n$), declines gradually and eventually vanishes for $P_n = P_{22}$. Consequently, at this limit ω falls to zero. For higher backpressure–and therefore higher secondary flow pressure –, the lower limit of (A_i/A_t) is accordingly further reduced.

The bottom border of the 3D-surface forms its intersection with the $\omega = 0$ plane and corresponds in Fig. 9(*b*) to the red "Upper Limit" curve. The calculations show that for a fixed value of backpressure (along a horizontal line in Fig. 9(*b*)), the Mach number M_a of the mixed stream *a,* first decreases, passes through a minimum, then increases and becomes at last equal to that of the primary flow at the nozzle exit. That means, the mixed gas mass flow rate reduces to that of the primary flow and hence, no secondary gas is entrained, *i.e.* $\omega = 0$. Concomitantly, the ejector area ratio (A_c/A_t) declines and reaches its minimum value at that limit. For ideal flow conditions (isentropic flow and ideal mixing of primary and secondary gas streams: $\eta_n = \eta_m = \eta_d = 1$), the ejector area ratio reduces, at that limit, to the nozzle area ratio,

$$(A_c/A_t)_{min} = A_n/A_t$$

The maximum value of ω on this line corresponds to the lowest Mach number M_a, $M_a = M_{22n}$. The deceleration of the gas in the mixing chamber (shrinkage of the Mach number of primary gas from M_{20n} to M_{22n}) corresponds to a maximum entrainment of secondary flow.

When, by applying fixed nozzle area ratio, backpressure is decreased, the evolution of the entrainment ratio follows a vertical line segment in Fig. 9(*b*), beginning on the red "Upper Limit" curve with $\omega = 0$ and ending on the "Lower Limit" curve with $\omega = 0$ again. Downwards along this line segment, ω increases first, reaches a maximum and then abruptly

falls to zero. In Fig. 8 just those branches of the ω *vs*. backpressure curves are depicted where the entrainment ratio is falling with a rising P_{23} (or T_{14}). More generally, on increasing the ejector backpressure, and consequently the secondary flow pressure, by fixing ejector geometry, a gradual reduction in entrainment ratio is caused.

The COP evolution *vs*. backpressure (or alternatively HP–generator temperature T_{14}) represented in Fig. 7 exhibits rather complex behaviour as it is conditioned by both the functioning of the double-effect chiller and the ejector behaviour. By increasing the backpressure P_{23}−and concomitantly the HP-generator temperature T_{14}− the COP tends first to increase even for a conventional double-effect absorption chiller however, the entrainment ratio in the considered pressure range (Fig. 8) falls. The global effect is thus first an increase of COP and then a decrease after passing a maximum corresponding to equal but antagonistic effects.

Finally, Fig. 10 represents the dependency of the entrainment ratio ω on the geometrical parameters of the ejector (A_n/A_t) and (A_c/A_t) in case #3 with driving steam temperature $T_{20} = 240ºC$ ($P_{20} = 33.4$ bar). It shows the limits of geometrical feasibility for the specified conditions and the evolution of the performance ω in this feasible geometric domain. It is worth mention that the feasible domain of the ejector design becomes narrow for higher entrainment ratios. The intersection of the light-green horizontal plane with the 3D-surface representing $\omega = f(A_n/A_t, A_c/A_t)$ gives the locus of design of a set of values for the geometrical parameters yielding the same entrainment ratio ($\omega = 0.3$ in Fig. 10). This curve is nearly linear; meaning that an increase of nozzle area ratio should be compensated by a proportional increase of ejector area ratio to maintain constant the entrainment ratio.

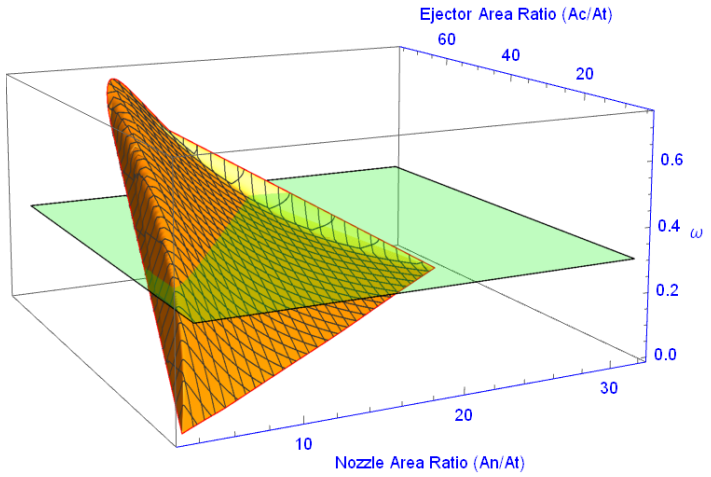

Figure 10. Entrainment ratio *vs*. nozzle area ratio and ejector ratio for case #3 at driving steam temperature $T_{20} = 240ºC$ ($P_{20} = 33.4$ bar)

6. Conclusions

An ejector driven double-effect absorption refrigeration cycle was presented and its energy performance discussed theoretically. In the water/lithium-bromide double-effect absorption cycle a steam ejector was incorporated in order to re-compress a fraction of the vapor leaving the HP–generator for re-heating the salt solution. Two alternative evaporation temperatures were considered (4°C or 12°C) and two scenarios for the cooling of condenser/absorber were discussed 35°C and 40°C. To drive the cycle, a high temperature heat source is required for generation of high-pressure steam.

Before running the simulations for the cycle configuration investigated in the present paper, the simulation tool was first tested and validated by comparing the calculated results with literature data whenever available. For the validation three tests were performed. First, the ejector sub-program was validated. Then, the simulation model was tested for an ejector driven single-effect absorption cycle. Finally, the main program was validated for a conventional double-effect absorption chiller without an ejector. The results predicted by the different parts of the simulation program are in good concordance with the data reported in the literature.

As regards the thermodynamic analysis of the double-effect absorption/recompression cycle, it is worthy of note that the cycle performance parameters are significantly affected by the presence and characteristics of the ejector, as the improvement of the COP largely depends on the entrainment ratio. Further, the COP responses to variation of working conditions were different from those observed for the conventional double-effect absorption refrigeration cycles. The most significant results are discussed in the following.

- The coefficient of performance (COP) of the ejector powered double-effect absorption/recompression cycle improved significantly as the driving steam temperature increased. At the operating conditions of the base case study, the COP-maximum occurred at HP-generator temperatures in the range of 120°C–125°C, lower by 20°C to 25°C than those for a maximum COP of the conventional double-effect absorption cycle. This maximum COP increased from 1.38 to 1.44 when the driving steam temperature was varied between 240ºC and 340ºC. At an HP-generator temperature of 135ºC, the enhancement factor of the COP was in the range 1.34 – 1.70 for the above mentioned interval of the driving steam temperature.
- COP − values responding to changes in HP–generator temperature were found to differ from those of the conventional double-effect absorption cycle. In particular, the COP increased with the heat source temperature T_{20} , even when the HP–generator temperature T_{14} remained unchanged. Moreover, at a constant temperature of the driving steam, the COP decreased just after reaching its maximum value when the HP−generator temperature increased.
- The ejector recompression technique affects the performance of the double-effect absorption refrigeration cycle in two ways: (i) eventual improvement of the COP and (ii) shift of the maximum COP to lower HP–generator temperatures in each case considered.
- The ejector powered double-effect absorption/recompression refrigeration cycle is a good configuration to make effective use of hot heat sources at a specific temperature range in an HP−generator. For instance, at an evaporator temperature of 12°C and a steam generator temperature of 320°C, the maximum COP of the ejector powered cycle is 1.57, *i.e.* 0.22 higher than that of the corresponding value for the double-effect absorption cycle at a condenser temperature of 35°C and 0.08 higher at a condenser temperature of 40°C with a $\mathrm{COP} = 1.35$.
- An efficient steam ejector is essential to obtain a high COP from the ejector powered cycle. The enhancement of the cycle performance due the presence of the ejector is however limited to a specific range of operating conditions and ejector geometry. Outside this range, the ejector is off-design. Furthermore, and this may be of practical importance, the larger the entrainment ratio desired, the narrower this feasible range of operation and geometrical parameters will be.

- Generally, the following requirements should be met to make the ejector powered cycle run efficiently. The ratio between the solution generator pressure (secondary flow of the ejector) and the steam pressure (primary flow of the ejector) should be kept as low as possible. The ejector geometry should be chosen for a maximum, practical, and feasible entrainment ratio.

Acknowledgements

Doniazed Sioud gratefully acknowledges the Tunisian Ministry of Higher Education and Scientific Research for funding her internships at Rovira i Virgili University of Tarragona (Spain).

Appendix

Simplified 1D mathematical ejector model

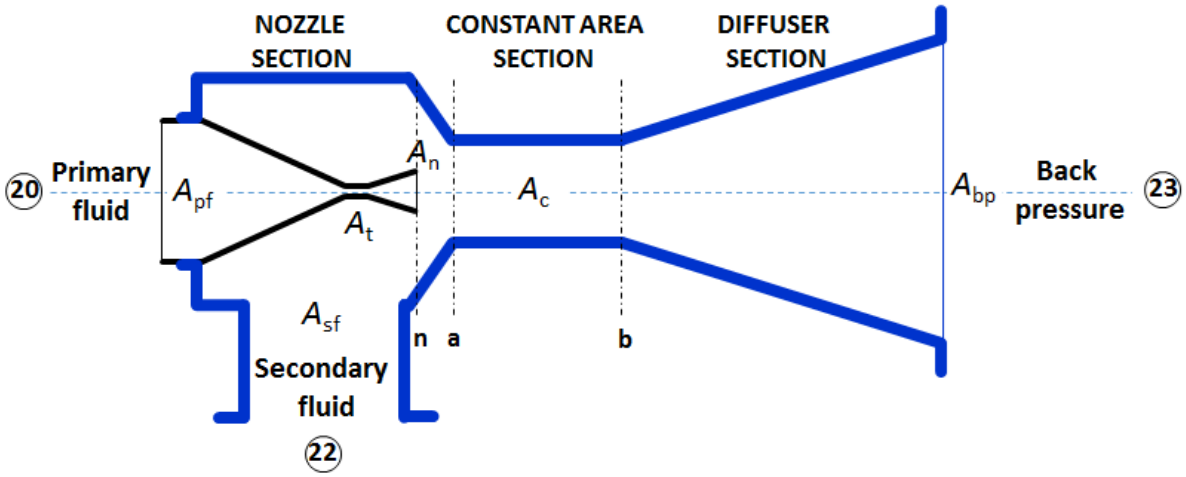

Figure A1. Schematic diagram of the ejector

The ejector performance is correlated to the entrainment ratio ω. To predict the ejector performance, the complicated flow and mixing problems within the ejector must be solved mathematically. The following simplified 1D–analysis is based on the assumptions:

- Primary and secondary fluids have comparable molecular weights and ratios of specific heat and are correctly described using the ideal gas model with constant specific heat.
- Primary fluid expands adiabatically in the nozzle, and mixture of primary and secondary fluid compresses adiabatically in the diffuser.
- Isentropic efficiencies, η_n and η_d, take into account friction losses in nozzle and diffuser.
- Inlet velocities of primary and entrained fluids are insignificant; velocity of the compressed mixture at ejector outlet is neglected.
- Mixing of primary and secondary fluids in the suction chamber occurs at constant pressure.

Governing equations

- The primary vapour (20) expands irreversibly through the nozzle. During this process, a portion of available energy is transformed into kinetic energy. Assuming an isentropic efficiency η_n, the velocity of the flow at the nozzle outlet (n) can be expressed in terms of the Mach number M_{20n} by applying the energy conservation,

$$\mathrm{M_{20n}} = \sqrt{\frac{2\,\eta_{\mathrm{n}}}{\gamma - 1}\left(\left(\frac{\mathrm{P_{20}}}{\mathrm{P_n}}\right)^{\frac{\gamma-1}{\gamma}} - 1\right)} \qquad (\mathrm{A}-1)$$

- The secondary vapour (22) expands reversibly in the suction chamber. Its velocity at the nozzle exit plane is expressed in terms of the Mach number $\mathrm{M}_{22\mathrm{n}}$ of the entrained fluid

$$\mathrm{M}_{22\mathrm{n}} = \sqrt{\frac{2}{\gamma - 1}\left[\left(\frac{\mathrm{P}_{22}}{\mathrm{P}_{\mathrm{n}}}\right)^{(\gamma-1)/\gamma} - 1\right]} \qquad (\mathrm{A}-2)$$

- The mixing process is modelled by 1D–continuity, momentum and energy equations. These equations are combined to define the critical Mach number M_a^* of the mixture at plane (a) in terms of the critical Mach number for the primary and entrained fluids at section (n),

$$\mathrm{M}_{\mathrm{a}}^* = \eta_{\mathrm{m}} \frac{\mathrm{M}_{20\mathrm{n}}^* + \omega\, \mathrm{M}_{22\mathrm{n}}^* \sqrt{\tau}}{\sqrt{(1+\omega\,\tau)(1+\omega)}} \qquad (\mathrm{A}-3)$$

M^* denotes the ratio of the local fluid velocity and the velocity of sound at critical conditions and $\tau = \frac{T_{22}}{T_{20}}$. The relation between both Mach numbers writes,

$$M = \sqrt{\frac{2\mathrm{M}^{*2}}{(\gamma+1) - (\gamma-1)\mathrm{M}^{*2}}} \qquad (\mathrm{A}-4)$$

- The Mach number, M_{a}, of the mixed stream can thus easily be calculated directly from M_a^*. In the constant area section (a)-(b) a sudden change of flow occurs from supersonic to subsonic conditions that simultaneously produce a rise in static pressure. The relation between the Mach numbers upstream and downstream of this shock wave is given by:

$$\mathrm{M}_{\mathrm{b}} = \sqrt{\frac{\frac{2}{\gamma-1} + \mathrm{M}_{\mathrm{a}}^2}{\frac{2\gamma}{\gamma-1}\mathrm{M}_{\mathrm{a}}^2 - 1}} \qquad (\mathrm{A}-5)$$

- The pressure increase across the shock wave is then

$$\frac{\mathrm{P}_{\mathrm{b}}}{\mathrm{P}_{\mathrm{a}}} = \frac{\mathrm{M}_{\mathrm{a}}}{\mathrm{M}_{\mathrm{b}}} \sqrt{\frac{1 + \frac{\gamma-1}{2}\mathrm{M}_{\mathrm{a}}^2}{1 + \frac{\gamma-1}{2}\mathrm{M}_{\mathrm{b}}^2}} \qquad (\mathrm{A}-6)$$

The constant pressure assumption implies $\mathrm{P}_{\mathrm{a}} = \mathrm{P}_{\mathrm{n}}$.

- The pressure lift in the diffuser is given by the relation

$$\frac{\mathrm{P}_{23}}{\mathrm{P}_{\mathrm{b}}} = \left(1 + \eta_{\mathrm{d}} \frac{\gamma-1}{2}\mathrm{M}_{\mathrm{b}}^2\right)^{\gamma/(\gamma-1)} \qquad (\mathrm{A}-7)$$

- Further, the nozzle throat and outlet area ratio is

$$\frac{A_n}{A_t} = \sqrt{\frac{1}{M_{20n}^2}\left(\frac{2}{\gamma+1}\left(1+\frac{\gamma-1}{2}M_{20n}^2\right)\right)^{(\gamma+1)/(\gamma-1)}} \qquad (A-8)$$

And the ratio of the nozzle throat area to the constant section area,

$$\frac{A_t}{A_c} = \sqrt{1-\left(\frac{P_b}{P_{23}}\right)^{(\gamma-1)/\gamma}}\ \frac{\left(\frac{\gamma-1}{2}\right)^{1/(\gamma-1)}}{\sqrt{(1+\omega\ \tau)(1+\omega)}}\ \frac{\left(\frac{P_{23}}{P_{20}}\right)\left(\frac{P_b}{P_{23}}\right)^{1/\gamma}}{\sqrt{1-\frac{2}{\gamma+1}}} \qquad (A-9)$$

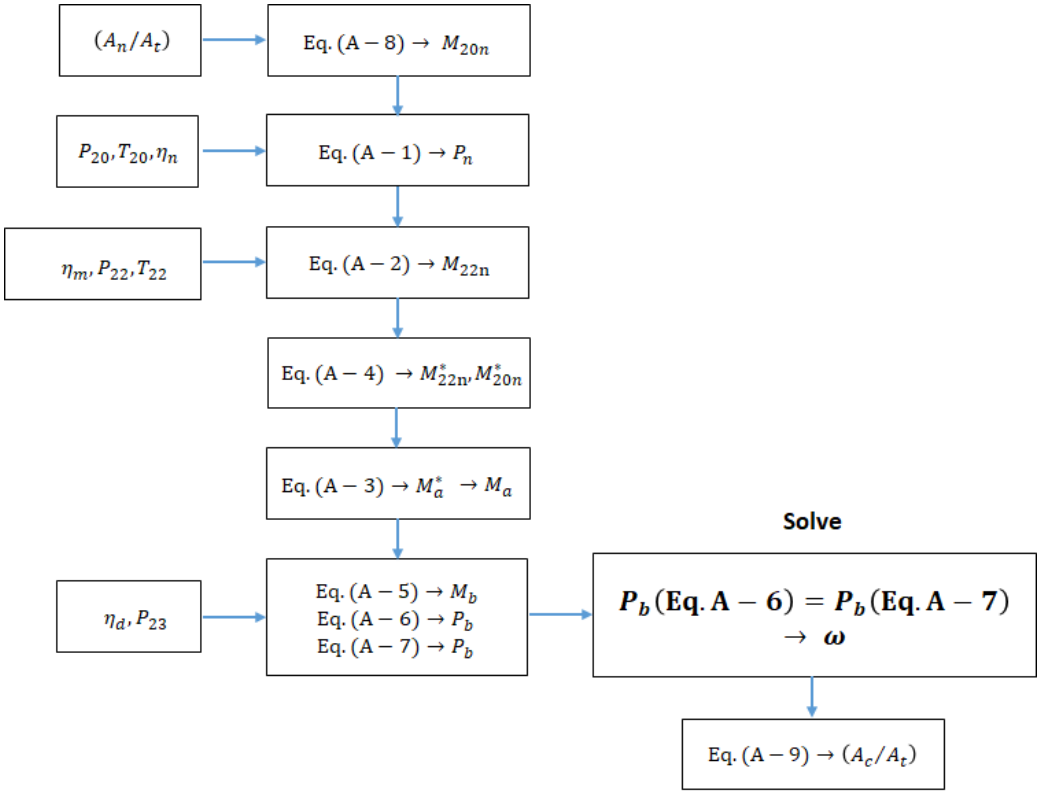

Figure A2. Solution procedure for ejector performance analysis

References

[1] Sun, D.W., Eames, I.W., Aphornratana, S., 1996. Evaluation of a novel combined ejector-absorption refrigeration cycle I: computer simulation. International Journal of Refrigeration, 19 (3), 172-180.

[2] Majdi, H.Sh., 2016. Performance evaluation of combined ejector LiBr/H2O absorption cooling cycle. Case Studies in Thermal Engineering, 7, 25–35.

[3] Jiang, L., Gu, Z., Feng, X. Li, Y, 2002. Study of new absorption-ejector hybrid refrigeration system. International Refrigeration and Air Conditioning Conference.

[4] Aphornratana, S., Eames, I.W., 1998. Experimental Investigation of a Combined Ejector-Absorption Refrigerator. International Journal of Energy Research, 22 (3), 195-207.

[5] Sirwan, R., Alghoul, M.A., Sopian, K., Ali, Y., Abdulateef, J., 2013. Evaluation of adding flash tank to solar combined ejector–absorption refrigeration system. Solar Energy, 91, 283-296.

[6] Abed, A.M., Alghoul, M.A., Sirawn,R., Al Shamani, A.N. Sopian, K., 2015. Performance enhancement of ejector-absorption cooling cycle by re-arrangement of solution streamlines and adding RHE, Applied Thermal Engineering, 77, 65-75.

[7] Shi, L., Yin, J., Wang, X., Zhu, M.S., 2001. Study on a new ejection-absorption heat transformer, Applied Energy, 68 (2), 161-171.

[8] Sözen, A., Özalp, M, 2003. Performance improvement of absorption refrigeration system using triple-pressure-level. Applied Thermal Engineering, 23 (13), 1577–1593.

[9] Vereda, C., Ventas, R., Lecuona, A., Venegas, M., 2012. Study of an ejector-absorption refrigeration cycle with an adaptable ejector nozzle for different working conditions. Applied Energy, 97, 305–312.

[10] Garousi Farshi, L., Mosaffa, A.H., Infante Ferreira, C.A., Rosen, M.A., 2014. Thermodynamic analysis and comparison of combined ejector–absorption and single-effect absorption refrigeration systems. Applied Energy, 133, 335–346.

[11] Eames, I.W., Wu, S., 2000. A theoretical study of an innovative ejector powered absorption-recompression cycle refrigerator. Intenational Journal of Refrigeration, 23 (6), 475-484.

[12] Eames, I.W., Wu, S., 2000. Experimental proof-of-concept testing of an innovative heat-powered vapour recompression-absorption refrigerator cycle, Applied Thermal Engineering, 20 (8), 721-736.

[13] Wu, S., Eames, I.W., 1998. A novel absorption-recompression refrigeration cycle, Applied Thermal Engineering, 18 (11), 1149-1157.

[14] Hong, D., Chen, G., Tang, L., He, Y., 2011. A novel ejector-absorption combined refrigeration cycle. International Journal of Refrigeration, 34 (7), 1596–1603.

[15] Farshi, L.G., Mahmoudi, S.M.S., Rosen, M.A., Yari, M., 2012. Use of low-grade heat sources in combined ejector–double effect absorption refrigeration systems. Journal of Power and Energy, 226 (5), 607–622.

[16] Grossman G., Wilk M., 1994. Advanced modular simulation of absorption systems, International Journal of Refrigeration, 17 (4), 231-244.

[17] Grossman G., Wilk M., 1993. Enhanced absorption cycle computer model. Oak Ridge National Laboratory, Oak Ridge-Tennessee 37831.

[18] Grossman G., Wilk M., Devault R.C., 1993. Simulation and performances analysis of triple-effect absorption cycle, ASHRAE winter meeting.

[19] Erickson D.C., Potnis S.V., Tang J., 1996. Triple effect absorption cycles – refrigeration heat pumps. In: Proceedings of the 31st Intersociety. Energy Conversion Engineering Conference (IECEC), 2, 1072–1077.

[20] Kim, J.S., Ziegler, F., Lee, H. 2002. Simulation of the compressor-assisted triple-effect H_2O/LiBr absorption cooling cycles. Applied Thermal Engineering, 22 (3), 295–308.

[21] Kaita, Y., 2002. Simulation results of triple-effect absorption cycles, International Journal of Refrigeration, 25 (7), 999 –1007.

[22] Gebreslassie, B.H., Medrano, M., Boer, D., 2010. Exergy analysis of multi-effect water–LiBr absorption systems: From half to triple effect. Renewable Energy, 35 (8), 1773–1782.

[23] Álvarez, M.E., Esteve, X., Bourouis, M., 2015. Performance analysis of a triple-effect absorption cooling cycle using aqueous (lithium, potassium, sodium) nitrate solution as a working pair. Applied Thermal Engineering, 79, 27-36.

[24] Azhar. Md., Siddiqui, M.A., 2013.thermodynamic analysis of a gas operated triple effect absorption cycle. International Journal of Innovative Research in Science, Engineering and Technology (ISSN), 2 (5), 1610- 1616.

[25] Shirazi, A., Taylor, R.A., White, S.D., Morrison, G.L., 2016. A systematic parametric study and feasibility assessment of solar-assisted single-effect, double-effect, and triple-effect absorption chillers for heating and cooling applications, Energy Conversion and Management, 114, 258–277.

[26] Lizarte, R., Marcos, J.D., 2016. COP optimisation of a triple-effect H_2O/LiBr absorption cycle under off-design conditions. Applied Thermal Engineering, 99, 195–205.

[27] Klein S.A., Alvarado F., 2005. Engineering equation solver, Version 7.441. Middleton, WI: F–chart software.

[28] Chen Y.M., Sun C.Y., 1997. Experimental study of the performance characteristics of a steam-ejector refrigeration system. Experimental Thermal and Fluid Science, 15 (4), 384-394.

[29] Huang, B.J., Chang, J.M., Wang, C.P. Petrenko, V.A., 1999. A 1-D analysis of ejector performance. International Journal of Refrigeration, 22 (5), 354–364.

[30] Somers, C., 2009. Modelling absorption chillers in aspen," simulation of absorption cycles for integration into refining processes", masters of science, University of Maryland, College Park, MD, USA.

List of Figures

Main text

Appendix

List of Tables